Backbone Dynamics of *trp* Repressor Studied by ^{15}N NMR Relaxation†

Zhiwen Zheng, Jerzy Czaplicki,‡ and Oleg Jardetzky*

Stanford Magnetic Resonance Laboratory, Stanford University, Stanford, California 94305-5055

Received November 21, 1994; Revised Manuscript Received February 2, 1995®

ABSTRACT: Backbone dynamics of *trp* repressor, a 25 kDa DNA binding protein, have been studied using ^{15}N relaxation data measured by proton-detected two-dimensional $^{1}H-^{15}N$ NMR spectroscopy. ^{15}N spin−lattice relaxation time (T_1), spin−spin relaxation time (T_2), and heteronuclear NOEs were determined for all visible backbone amide ^{15}N nuclei. Monte Carlo simulations of the amplitudes of backbone motions led to the conclusion that a wobbling in a cone model with consideration of the anisotropic reorientation of the molecule was appropriate to describe the underlying motions, allowing us to derive the semiangle of the cone (α) and the effective correlation time for internal motions (τ_e) for each N−H bond vector. The final optimized rotational diffusion coefficients parallel ($D_{\parallel}$) and perpendicular ($D_{\perp}$) to the unique axis of the molecule were found to be $1.48 \pm 0.06 \times 10^7$ and $1.15 \pm 0.05 \times 10^7$ s^{-1}, respectively. The average semiangle of the cone (α) describing the amplitude of NH vector motions on the picosecond time scale was found to be $20.9 \pm 5.7°$. Large amplitude motions on the picosecond time scale are found at both the N and C termini but are restricted in both the hydrophobic core and DNA-binding regions.

The problem of molecular recognition mechanisms for DNA-binding proteins has been in the focus of attention for some time. Recent years have witnessed many efforts to define the relationships between structural features of a protein and its DNA-binding properties (Pabo & Sauer, 1992). In some cases, however, notably in the case of the *trp* repressor, it has become apparent that the dynamics of the protein molecule may play an equally important role in the binding process (Arrowsmith et al., 1991a; Czaplicki et al., 1991; Zhao et al., 1993; Zhang et al., 1994, Gryk et al., 1995). The work reported here is aimed at a further elucidation of the molecular dynamics of the *trp* repressor and of the dynamic features necessary for binding of the protein to DNA.

The *trp* repressor from *Escherichia coli* is a 25 kDa allosteric protein, regulating the biosynthesis of L-tryptophan (Klig et al., 1988; Luisi & Sigler, 1990). In the absence of L-Trp the *trp* repressor molecules (aporepressor) have a low affinity for DNA, while in its presence (holorepressor) they form a stable complex with DNA, inhibiting the production of enzymes involved in tryptophan biosynthesis. The *trp* repressor molecules in solution form symmetric dimers with 107 residues per monomer. Both the crystal structures (Schevitz et al., 1985; Zhang et al., 1987; Otwinowski et al., 1988) and the NMR solution structures (Arrowsmith et al., 1989, 1990, 1991a,b; Zhao et al., 1993) of the *trp* repressor and of its complex with DNA (Zhang et al., 1994) are known. The molecule contains six helices per monomer, denoted as ABCDEF, four of which (ABCF) constitute the hydrophobic core of the molecule, while the remaining two (DE) form the helix−turn−helix DNA binding region.

We have used inverse-detected two-dimensional $^{1}H-^{15}N$ NMR experiments to examine the backbone dynamics of *trp* repressor. Different methods were tried in analyzing the amide ^{15}N relaxation data, and by comparing the results of each analysis to molecular dynamics (MD) simulations and Monte Carlo (MC) exploration of the accessible conformational space for backbone motions, it was found that the relaxation data can be best analyzed using a wobbling in a cone model (King et al., 1978; Howarth, 1978, 1979) with the consideration of the anisotropic reorientation of the molecule. The model provides a clear physical picture of the motions allowed in MD and MC simulations, and the internal motions can be interpreted in terms of the semiangles of the cone (α) and the effective correlation time for internal motions (τ_e) for each N−H bond vector.

METHODS

Sample Preparation. The uniformly ^{15}N-enriched *trp* repressor was isolated from *E. coli* strain CY15070 containing the overproducing plasmid pJPR2 (Paluh & Yanovsky, 1986). The strain was grown in M9 minimal medium with $[^{15}N]NH_4Cl$ (99 atom % ^{15}N, Isotec Inc.) as the sole nitrogen source. The cell growth conditions and protein purification procedures have been described previously (Gryk et al., 1995). The protein was then concentrated to 4.6 mM (in terms of protein monomer) in the NMR buffer (500 mM NaCl, 50 mM NaH_2PO_4, 90% H_2O/10% D_2O). The NMR sample of holorepressor was finally obtained by adding a 3-fold molar excess of L-tryptophan into the aporepressor solution. The sample with the solution pH found to be 7.2 was used for the ^{15}N T_1, T_2, and $\{^{1}H\}-^{15}N$ NOE measurements. The NOE experiments were repeated with the same sample at pH 6 titrated by adding less than 5 μL of 1 M HCl (the changes in the protein concentration upon titration should be negligible).

NMR Spectroscopy. All NMR experiments were recorded at 500.13 MHz (^{1}H) and 50.68 MHz (^{15}N) on a Bruker AM-500 spectrometer equipped with Aspect 3000 computer and

† This work is supported by NIH Grants GM33385 and RR07558.

* Correspondence author (telephone, 415-723-6270; Fax, 415-723-2253; Email, jardetzky@camis.stanford.edu).

‡ Current address: Centre de Recherche de Biochimie et Génétique Cellulaires, CNRS, 118, route de Narbonne, 31062 Toulouse Cedex, France (Email: cgeorge@lptf.biotoul.fr).

® Abstract published in *Advance ACS Abstracts,* April 1, 1995.

0006-2960/95/0434-5212$09.00/0

FMR decoupler tuned to the ^{15}N frequency. All measurements were carried out at 318 K. The ^{1}H-detected pulse sequences used to measure ^{15}N T_1 and T_2 relaxation times and $\{^{1}H\}-^{15}N$ NOEs were based on those described previously by Barbato et al. (1992). All experiments were collected with a spectral width of 6493.5 Hz in the F_2 domain and 3012.1 Hz in the indirectly detected F_1 domain. Quadrature detection in F_1 was achieved by using time-proportional phase incrementation (TPPI) (Marion & Wuthrich, 1983). The ^{1}H carrier frequency was set to the water resonance, and the water signal in all experiments was suppressed by low-power presaturation. Time domain data were recorded with 1024 complex points in t_2 and with 256 points in the t_1 dimension; 128 scans per t_1 increment were acquired for T_1 experiments, while 200 scans per t_1 increment were accumulated for both T_2 and heteronuclear NOE experiments. The 90° pulse widths were 15 μs for ^{1}H and 60 μs for ^{15}N. ^{15}N decoupling during t_2 acquisition time was carried out using WALTZ-16 decoupling (Shaka et al., 1983).

For T_1 and T_2 experiments, a relaxation delay of 1.0 s was used between acquisitions. For NOE experiments, a relaxation delay of 3.0 s was used to ensure the maximal development of NOEs before acquisition. The time interval between the refocusing pulses in the Carr−Purcell−Meiboom−Gill (CPMG) (Carr & Purcell, 1954; Meiboom & Gill, 1958) period of the T_2 experiments was set to 0.5 ms to effectively spin-lock the heteronuclear spins. Ten delays of 40, 100, 200, 400, 600, 800, 1000, 1200, 1500, and 2000 ms were used during the perturbation−recovery period of the T_1 experiments, whereas delays of 4.5, 9.1, 18.2, 29.6, 45.5, 68.2, 100.1, and 150.1 ms were used during the CPMG period of the T_2 experiments.

All spectra were processed on a Silicon Graphics Iris Indigo workstation using the FELIX NMR data processing package developed by Hare Research. The residual water peak was removed by convolution of the signal, and the time domain data were zero-filled to 1024 and 512 real points in the t_1 and t_2 dimensions, respectively, and apodized using a sine-bell squared window shifted by 45° before Fourier transformation was performed in both frequency dimensions. Polynomial baseline corrections were applied in the F_2 domain after Fourier transformation. Previously published amide proton/nitrogen assignments (Arrowsmith et al., 1990; Czaplicki et al., 1991; Borden et al., 1992; Ramesh et al., 1994) were used. Chemical shifts were measured relative to the Ala 29 resonance with 8.95 ppm in the ^{1}H dimension and 126.90 ppm in the ^{15}N dimension, while a total of 71 residues were assigned.

The ^{15}N T_1 and T_2 relaxation times were determined from nonlinear least squares fits of the experimental peak intensities to two-parameter single exponential functions. The Marquardt nonlinear least squares routine (Press et al., 1989), which combines the inverse Hessian method and the steepest descent method, was used in this study. Uncertainties in the calculated relaxation time were determined from the covariance matrix.

Analysis of T_1, T_2, and NOE Data. The spin relaxation of the protein backbone amide ^{15}N nucleus is dominated by the dipolar interaction between the ^{15}N nucleus and the attached ^{1}H nucleus, as well as the chemical shift anisotropy (CSA). The ^{15}N longitudinal (T_1) and transverse (T_2) relaxation times and the heteronuclear NOEs are given by combinations of the five spectral density functions, $J(\omega)$, listed as follows (Abragam, 1961):

$$\frac{1}{T_1} = d^2[J(\omega_H - \omega_N) + 3J(\omega_N) + 6J(\omega_H + \omega_N)] + c^2J(\omega_N) \quad (1)$$

$$\frac{1}{T_2} = \frac{d^2}{2}[4J(0) + J(\omega_H - \omega_N) + 3J(\omega_N) + 6J(\omega_H) + 6J(\omega_H + \omega_N)] + \frac{c^2}{6}[4J(0) + 3J(\omega_N)] \quad (2)$$

$$\mathrm{NOE} = 1 + d^2\left(\frac{\gamma_H}{\gamma_N}\right)[6J(\omega_H + \omega_N) - J(\omega_H - \omega_N)]T_1 \quad (3)$$

in which

$$d^2 = 0.1\gamma_H{}^2\gamma_N{}^2\left(\frac{h}{2\pi}\right)^2\langle r_{NH}{}^{-3}\rangle^2 \quad (4)$$

$$c^2 = \frac{2}{15}\omega_N{}^2(\sigma_{||} - \sigma_\perp)^2 \quad (5)$$

where h is Planck's constant ; γ_H and γ_N are the gyromagnetic ratios of ^{1}H and ^{15}N, and ω_H and ω_N are the Larmor frequencies of ^{1}H and ^{15}N nuclei, respectively; r_{NH} is the $^{1}H-^{15}N$ internuclear distance (r_{NH} = 1.0 Å); $\sigma_{||}$ and $\sigma_\perp$ are the parallel and perpendicular components of the axially symmetric ^{15}N chemical shift tensor, and $(\sigma_{||} - \sigma_\perp) = -160$ ppm (Hiyama et al., 1988).

The spectral density depends on the overall motion of the protein as a whole as well as on the internal motions of each $^{1}H-^{15}N$ bond vector. From the three experimental measurements, T_1, T_2, and NOE, we cannot determine the spectral density at five frequencies in eq 1−3 independently, but for our purpose of obtaining physical insight into the underlying motions, this is in fact not necessary. An appropriate model has to be used to correlate the spectral density functions to the molecular microscopic dynamic parameters, whether one is fitting the measured relaxation parameters or the precalculated spectral density functions. The choice of the model depends on information not obtainable from an NMR experiment but can be greatly facilitated by the results of molecular dynamics simulations.

To begin with, we note that the *trp* repressor protein is highly asymmetric. The analysis of the atomic coordinates of a set of solution structures (Zhao et al., 1993) yields an average axial ratio of 1.6:1.15:1. This result clearly indicates that the shape of this molecule should be approximated by an anisotropic ellipsoid rather than a sphere. The longest axis is found to be nearly parallel to helix C of both monomers. The lengths of the other two axes are comparable, so that a prolate ellipsoid of revolution can be used as a first approximation.

For a totally anisotropic molecule, the spectral density function is related to the three rotational diffusion coefficients, D_{xx}, D_{yy}, and D_{zz}, along three principal axes of the molecule and is given by Woessner (1962a):

$$J(\omega) = C_1\frac{\tau_1}{1+\omega^2\tau_1^2} + C_2\frac{\tau_2}{1+\omega^2\tau_2^2} + C_3\frac{\tau_3}{1+\omega^2\tau_3^2} + C_+\frac{\tau_+}{1+\omega^2\tau_+^2} + C_-\frac{\tau_-}{1+\omega^2\tau_-^2} \quad (6)$$

The correlation times τ_i are functions of the diffusion coefficients, while the diffusion coefficients C_i depend additionally on the direction cosines of the internuclear vectors in the molecular frame. These can be calculated when the atomic coordinates are known, but for the sake of brevity we shall not give the explicit expressions here [for an extensive review, see Kitamaru (1986)].

For an axially symmetric molecule with only two rotational diffusion coefficients parallel ($D_\parallel$) and perpendicular ($D_\perp$) to the unique axis of the molecule, the expressions for calculating the spectral densities can be simplifed from eq 6 and is given by Woessner (1962b):

$$J(\omega) = C_1\frac{\tau_1}{1+\omega^2\tau_1^2} + C_2\frac{\tau_2}{1+\omega^2\tau_2^2} + C_3\frac{\tau_3}{1+\omega^2\tau_3^2} \quad (7)$$

with

$$C_1 = \frac{3}{4}\sin^4\theta \quad (8a)$$

$$C_2 = 3\sin^2\theta\cos^2\theta \quad (8b)$$

$$C_3 = \frac{1}{4}(3\cos^2\theta - 1)^2 \quad (8c)$$

where θ is the angle between the N−H internuclear vector and unique axis of the molecule. The correlation times τ_1, τ_2, and τ_3 depend on the rotational diffusion coefficients:

$$\tau_1 = \frac{1}{4D_\parallel + 2D_\perp} \quad (9a)$$

$$\tau_2 = \frac{1}{D_\parallel + 5D_\perp} \quad (9b)$$

$$\tau_3 = \frac{1}{6D_\perp} \quad (9c)$$

To take internal motions into account, we have explored several alternatives, discussed under Results and Discussion. On the basis of MD and MC simulations of backbone motions, obtained in the course of structure refinement (Zhao et al., 1993), we concluded that the "wobbling in a cone" model (King et al., 1978; Howarth, 1978, 1979) adequately describes the allowed motions of the NH vector. This model assumes that each internuclear vector librates in the cone while it also reorients along the whole molecule. Such a model provides a clear physical picture of the allowed range of internal motions and requires a minimum number of parameters. For a spherical molecule, the spectral density can be expressed in terms of the correlation time for the whole molecule, τ_{iso}, the semiangle of the wobbling cone, α, and the librational correlation time, τ_e, for each NH vector.

$$J(\omega) = A\frac{\tau_{iso}}{1+(\omega\tau_{iso})^2} + (1-A)\frac{\tau_p}{1+(\omega\tau_p)^2} \quad (10)$$

where

$$A = \left[\frac{1}{2}(\cos\alpha)(1+\cos\alpha)\right]^2 \quad (11)$$

and

$$\frac{1}{\tau_p} = \frac{1}{\tau_{iso}} + \frac{1}{\tau_e} \quad (12)$$

In this case, the coefficient A, which reflects the amplitude of internal motion for each internuclear vector, is identical to the order parameter, S^2, of the "model-free" model proposed by Lipari and Szabo (1982a,b):

$$S^2 = A \quad (13)$$

In the case of anisotropic rotation with internal motion, the calculation of the spectral density function can be based on a combination of eq 6 or 7 and eq 10 and 11. On the very general assumption that the anisotropic and internal motions are independent Markov processes, it has been shown that the spectral density function will be given by a sum of appropriate Lorentzians, and even in the case of coupled motions the sum remains a good approximation (King & Jardetzky, 1978; Lipari & Szabo, 1982a), i.e., in the general case:

$$J(\omega) = A\left[C_1\frac{\tau_1}{1+\omega^2\tau_1^2} + C_2\frac{\tau_2}{1+\omega^2\tau_2^2} + C_3\frac{\tau_3}{1+\omega^2\tau_3^2} + C_+\frac{\tau_+}{1+\omega^2\tau_+^2} + C_-\frac{\tau_-}{1+\omega^2\tau_-^2}\right] + (1-A)\left[C_1\frac{\tau_1'}{1+\omega^2\tau_1'^2} + C_2\frac{\tau_2'}{1+\omega^2\tau_2'^2} + C_3\frac{\tau_3'}{1+\omega^2\tau_3'^2} + C_+\frac{\tau_+'}{1+\omega^2\tau_+'^2} + C_-\frac{\tau_-'}{1+\omega^2\tau_-'^2}\right] \quad (14)$$

where

$$\frac{1}{\tau_i'} = \frac{1}{\tau_i} + \frac{1}{\tau_e}, \quad \tau_i = \tau_1, \tau_2, \tau_3, \tau_+, \tau_- \quad (15)$$

For an axially symmetric molecule we will have

$$J(\omega) = A\left[C_1\frac{\tau_1}{1+\omega^2\tau_1^2} + C_2\frac{\tau_2}{1+\omega^2\tau_2^2} + C_3\frac{\tau_3}{1+\omega^2\tau_3^2}\right] + (1-A)\left[C_1\frac{\tau_1'}{1+\omega^2\tau_1'^2} + C_2\frac{\tau_2'}{1+\omega^2\tau_2'^2} + C_3\frac{\tau_3'}{1+\omega^2\tau_3'^2}\right] \quad (16)$$

with C_1, C_2, and C_3 given by eq 8a−c and the correlation times τ_1, τ_2, and τ_3 by eq 9a−c. Again the correlation times, τ_1', τ_2', and τ_3', depend on fast internal motions and are functions of the internal rotational correlation time as well as of the correlation times of the overall molecular motion, i.e.

$$\frac{1}{\tau_i'} = \frac{1}{\tau_i} + \frac{1}{\tau_e}, \quad \tau_i = \tau_1, \tau_2, \tau_3 \tag{17}$$

RESULTS AND DISCUSSION

T_1, T_2, and NOE Relaxation Data. Contour plots of the $^1H-^{15}N$ correlation spectra of *trp* repressor are presented in Figure 1 for the ^{15}N T_1 (A) and T_2 (B) experiments at three different interval times T. Typical T_1 and T_2 relaxation data and fitted curves are shown in Figure 2 for residues A29, L71, and D108. These residues are located in the hydrophobic core, in the DNA-binding region, and on C termini, respectively. The NOE experiments were performed with the same sample at both pH 7.2 and pH 6 to examine the effect of solvent presaturation on the NOE measurements. The average deviation between the two set NOEs from their mean values was found to be 5.1% for amides in the ABCF core region and to be 15.4% in the DE DNA-binding region, indicating that the solvent presaturation does not have significant effect on the NOE measurements. The average NOEs between the two sets as well as T_1 and T_2 relaxation times are shown in Figure 3. Except in residues on both N and C termini, the T_1, T_2, and NOE do not exhibit much variation from residue to residue. The mean relaxation times T_1 and T_2 were 789 ± 65 ms and 63.3 ± 40 ms, respectively. Only residue D108 was found to have both T_1 and T_2 that are significantly larger than the corresponding mean values. T_2 for residue K106 is larger than the mean value by about one standard deviation. The mean NOE was found to be 0.66 ± 0.38. Only residues M11 and D108 show negative NOEs, and K106 has an NOE that is much smaller than the mean value. Note that resonance peaks for residues M11, S67, I79, and V94 only appear in the spectra of NOE experiments measured at pH 6 because the amide protons for these residues have very fast solvent exchange rates (Gryk et al., 1995) at pH 7.2. Excluding residues M11, K106, and D108, the mean values for T_1, T_2, and NOEs were found to be 783 ± 43 ms, 62 ± 7 ms and 0.73 ± 0.06, respectively. These results clearly show that on the nanosecond time scale the *trp* repressor is quite rigid along its entire backbone except at the two termini.

Calculation of the Anisotropy from Models of the trp Repressor. It is well-known (Perrin, 1934) that the overall molecular motion is quite dependent on the physical shape of the molecule which, for *trp* repressor, we can examine from the known solution structures. A family of ~30 individual solution structures of the *trp* repressor molecule calculated in this laboratory on the basis of NOE data was used to find the lengths and orientations of the principal axes of the molecule. The details of the strategy responsible for generating the structures have been published elsewhere (Zhao et al., 1993; Zhao & Jardetzky, 1993). The coordinate system of each structure was translated to the center of mass of the molecule, and then the components of the mass distribution were calculated from

$$I_{ij} = \frac{\sum_{k=1}^{N} m_k q_{ki} q_{kj}}{\sum_{k=1}^{N} m_k} \tag{18}$$

where m_k is the mass of kth atom and q_{ki} is its ith coordinate. After diagonalization the eigenvalues allow us to determine the lengths of the semiaxes $a_i = I_{ij}^{1/2}$, while the eigenvectors give orientations of the principal axes of the molecule with respect to the frame in which calculations are performed. The average axial ratios found by this procedures were 1.6:1.15:1 from the solution structures. The axial ratios calculated from the crystal structure of Zhang et al. (1987) were found to be 1.58:1.2:1. Next, we rotate the coordinate system to the principal axes system, since it facilitates finding direction cosines of individual NH vectors, necessary for computing the spectral density functions. For each residue the direction cosines of NH vectors obtained from all NMR structures were averaged, and the angles between each averaged NH vector and the longest axis are displayed in Figure 4A as a function of residue number. It is seen that the NH vector direction angles have quite distinctive values from one helix to the other. The NH vectors in helix C have the smallest angles, very much parallel to the longest axis of the molecule. In contrast, those NH vectors in helixes A, B, and F have very large angles with respect to the longest axis. The angles for residues in the D and E helix region vary in a very wide range.

Experimental Estimate of the Motional Anisotropy from the T_1/T_2 Ratio. The large axial ratio between the principal axis of *trp* repressor found in the solution structures strongly suggests that the overall motion of the molecule may exhibit anisotropic reorientation. Such a motional anisotropy should be also reflected in the ^{15}N relaxation experimental data. From eq 1−5, the T_1 and T_2 relaxation times are functions not only of the overall rotational correlation times but also of those for the rapid internal motions (on the time scale τ_e). If the amplitudes of internal motions are small ($(1 - A) < 0.3$), however, as discussed previously by Kay et al. (1989), the effect of rapid motions cancels out when the overall rotational correlation times are calculated from the T_1/T_2 ratio. This is because, to a first approximation, the second term in the spectral density equations (eq 10, 14, and 16) can be dropped out and the fast internal motions lengthen both T_1 and T_2 values by the same factor, A. The experimental ^{15}N T_1/T_2 ratio as a function of residue number is presented in Figure 4B, designated by open diamonds. Compared with the angles of the NH vectors with respect to the molecular principal axis as shown in Figure 4A, it is not difficult to see that there is a clear correlation between the NH vector direction angles and the T_1/T_2 ratio. The T_1/T_2 ratios for helix C, where NH vectors have relatively smaller direction angles, are greater than those in the helix A, B, and F regions. This is quite reasonable for a macromolecule since T_1 values increase with the decrease in the overall tumbling rate, while the effect of overall motion on T_2 values is the opposite. The NH dipolar vectors parallel to the longest principal axis of the molecule reorient at a slower rate than vectors perpendicular to it. Therefore, the ^{15}N T_1/T_2 ratio for residues in helix C is expected to be greater than for residues in other regions.

When using the T_1/T_2 ratio to determine the overall correlation times, certain precautions must be taken (Kay et al., 1989). Residues that have a strong heteronuclear NOE effect (NOE < 0.65) should be excluded from the calculation, since in this case fast internal motions are likely to make significant contributions to the T_1, T_2 relaxation times. Residues for which T_2 values are drastically shortened by exchange should also be excluded from the calculation. We

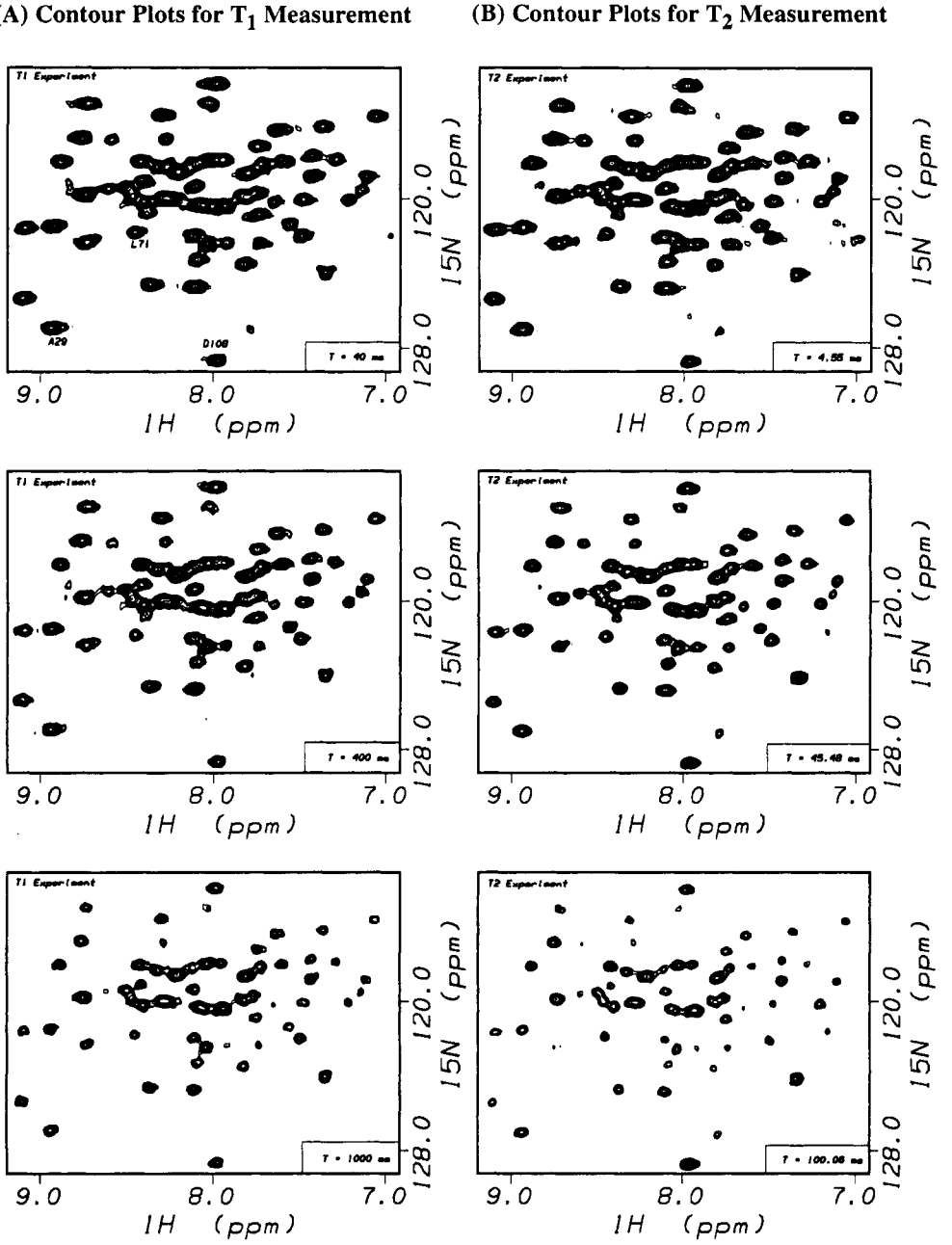

FIGURE 1: Contour plots of the $^1H-^{15}N$ correlation spectra of *trp* repressor for the ^{15}N T_1 (A) experiment with interval times equal to 40, 400, and 1000 ms and T_2 (B) experiments with interval times equal to 4.55, 45.48, and 100.06 ms.

therefore exclude residues in helices D and E, since the observed rapid amide/solvent proton exchange rates in this region (Czaplicki et al., 1991; Gryk et al., 1995) may cause errors in the T_2 measurement. The overall rotational diffusion coefficients, D_{xx}, D_{yy} and D_{zz}, were determined by minimizing the following sum of squared difference function $Y(D_{xx},D_{yy},D_{zz})$:

$$Y(D_{xx},D_{yy},D_{zz}) = \sum_i \left[\left(\frac{T_1}{T_2}\right)_{\text{calc},i} - \left(\frac{T_1}{T_2}\right)_{\text{expt},i}\right]^2 \quad (19)$$

where the index i refers to the ith residue used in the calculation (the total number of residues used was 47). The subscript "expt" refers to the experimental value. The subscript "calc" refers to the calculated values based on eq 1−5 and 14. Note that to a first approximation the calculated T_1/T_2 ratio is no longer related to internal motions (A and τ_e are not included in the function):

$$\left(\frac{T_1}{T_2}\right)_{\text{calc},i} = f(D_{xx},D_{yy},D_{zz},l_i,m_i,n_i) \quad (20)$$

where the direction cosines l_i, m_i, and n_i for the NH vector of the ith residue were determined from the solution structures. To choose a best model for the overall motion from the experimental data, the minimization procedures were performed for the following three cases: (i) optimizing one variable parameter D_{xx} by locking $D_{yy} = D_{zz} = D_{xx}$ (isotropic rotation); (ii) optimizing two variable parameters D_{xx} and D_{yy} by locking $D_{zz} = D_{yy}$ with D_{xx} along the longest principal axis of the molecule (axially symmetric rotation); (iii) optimizing the three rotational diffusion coefficients with no restriction between them (totally anisotropic rotation). A routine using conjugate gradient methods (Press et al., 1989)

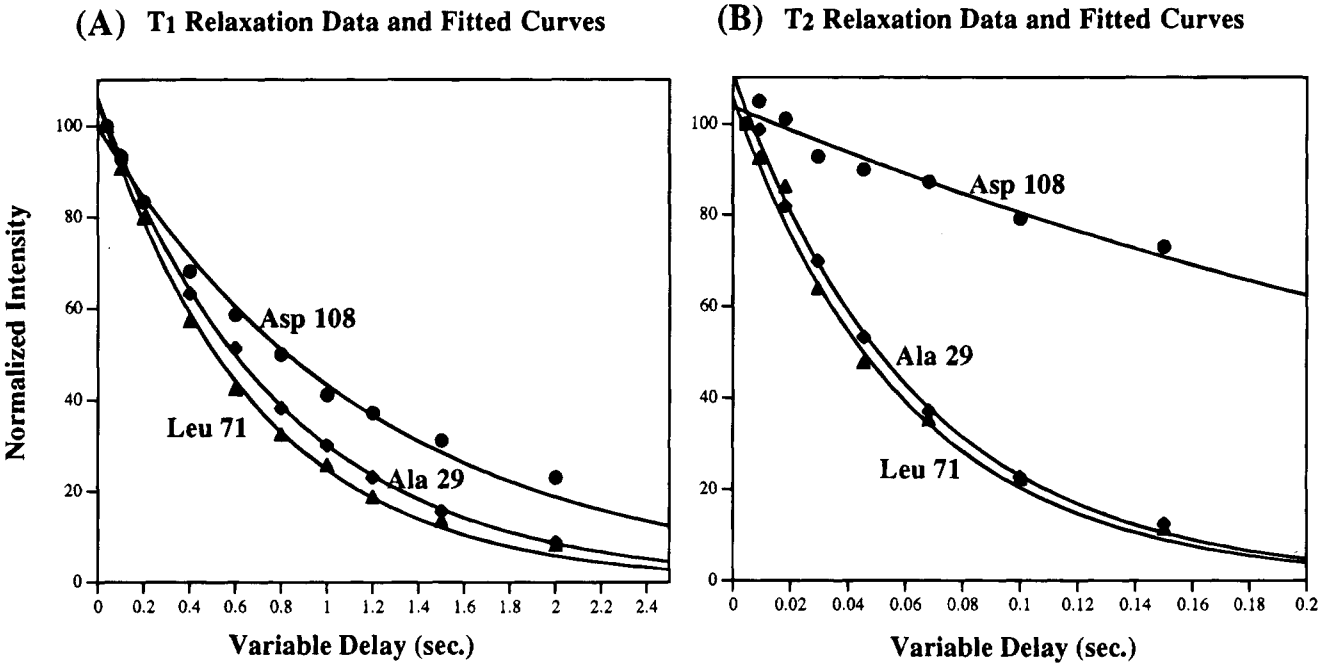

FIGURE 2: Experimental T_1 (A) and T_2 (B) relaxation data points and fitted curves for the three residues Ala 29 (◆), Leu 71 (▲), and Asp 108 (●) in three distinctive regions of *trp* repressor.

was applied in the minimization procedure. The minimized Y function values for the three cases were found to be 86.90, 47.54, and 47.34, respectively. The Y value for the isotropic tumbling model is almost twice as large as that for the anisotropic motional models. On this basis, the isotropic rotational model can be rejected from further consideration. The Y values for cases ii and iii are almost identical. Statistically, the choice of models can be made by comparing the Y value divided by the degrees of freedom $(N - M)$, where N is the total number of experimental T_1/T_2 values used in the calculation and M is the number of variable parameters. The axially symmetric rotation was chosen as an adequate model for describing the overall motion of *trp* repressor since its $Y/(N - M)$ value is the smallest among the three cases. Using the axially symmetric rotational model, the optimized rotational diffusion coefficients parallel $(D_{\parallel})$ and perpendicular $(D_{\perp})$ to the unique axis of the molecule were found to be $1.48 \pm 0.06 \times 10^7$ s^{-1} and $1.15 \pm 0.05 \times 10^7$ s^{-1}, respectively. The calculated T_1/T_2 ratio using the optimized parameters as a function of residue number is also presented in Figure 4B, designated by the filled diamonds. It is not difficult to see from Figure 4B that reasonably good agreement is obtained between the experimental and calculated T_1/T_2 values. The axes of the rotational diffusion tensor are shown in Figure 5, with reference to the solution structure determined in this laboratory.

Evaluation of Internal Motion for Each N−H Vector. In the last section, the overall rotational diffusion coefficients were determined regardless of the existence of the internal motions. If the molecule is really a rigid rotor, the calculated T_1, T_2, and NOE based on eq 1−5 and 7, excluding the internal rotation contributions (i.e., setting $A = 1$ in eq 16), should be consistent with the measured values. Using the rigid rotor model and predetermined $D_{\parallel}$ and $D_{\perp}$ values, the calculated ^{15}N T_1, T_2, and NOE were found on average over the protein backbone to be 661 ± 26 ms, 51 ± 2 ms, and 0.808 ± 0.001, respectively. Both T_1 and T_2 are less than the measured T_1, T_2 values (783 ± 43 ms and 62 ± 7 ms, respectively), and NOEs are greater than those measured (0.73 ± 0.06). Such discrepancies indicate that the contributions from the fast internal motions, which will lengthen both T_1 and T_2 relaxation times and reduce NOE values, cannot be completely ignored in the relaxation data analysis. It should be noted that varying $D_{\parallel}$ and $D_{\perp}$ cannot account for the T_1, T_2 discrepancies between the calculated and measured values because the effect of overall motion changes T_1 and T_2 in opposite ways.

In order to gain more insight into the nature of physical processes involved in internal motions, we decided to follow the spatial trajectories of NH vectors. For each residue in the amino acid sequence of the *trp* repressor molecule, the orientation of its NH vector in the molecular principal frame was calculated from each of the available solution structures, refined by an MD sequential simulated annealing protocol. In addition, an MD−MC selection (Zhao & Jardetzky, 1995) was carried out. As a result, for each residue in the backbone we obtained a family of vectors representing variations of their orientations. Plotting the coordinates of the tips of these vectors in the plane perpendicular to the direction of the average vector gives us a cross-sectional view of the distribution of the allowed orientations, containing all allowed orientations of the NH vectors. On the basis of the ergodic theorem we may regard this family of structures as a representation of the time evolution of one individual structure (Zhao & Jardetzky, 1993). Hence, the family of NH vectors of a given residue may be regarded as an approximate representation of the motion of this vector. Figure 6 presents six typical examples, illustrating patterns from each of the six helices. For most residues in any part of the molecule, the NH vectors predominantly form a cone or a cone whose cross sections are ellipsoidal. For very few residues the NH trajectories resemble a fan (not shown). This allows us to adopt the wobbling in a cone model of Howarth (1979) to represent the motion of internuclear NH vectors in the *trp* repressor molecule. As noted above for the isotropic case, this model is mathematically equivalent to

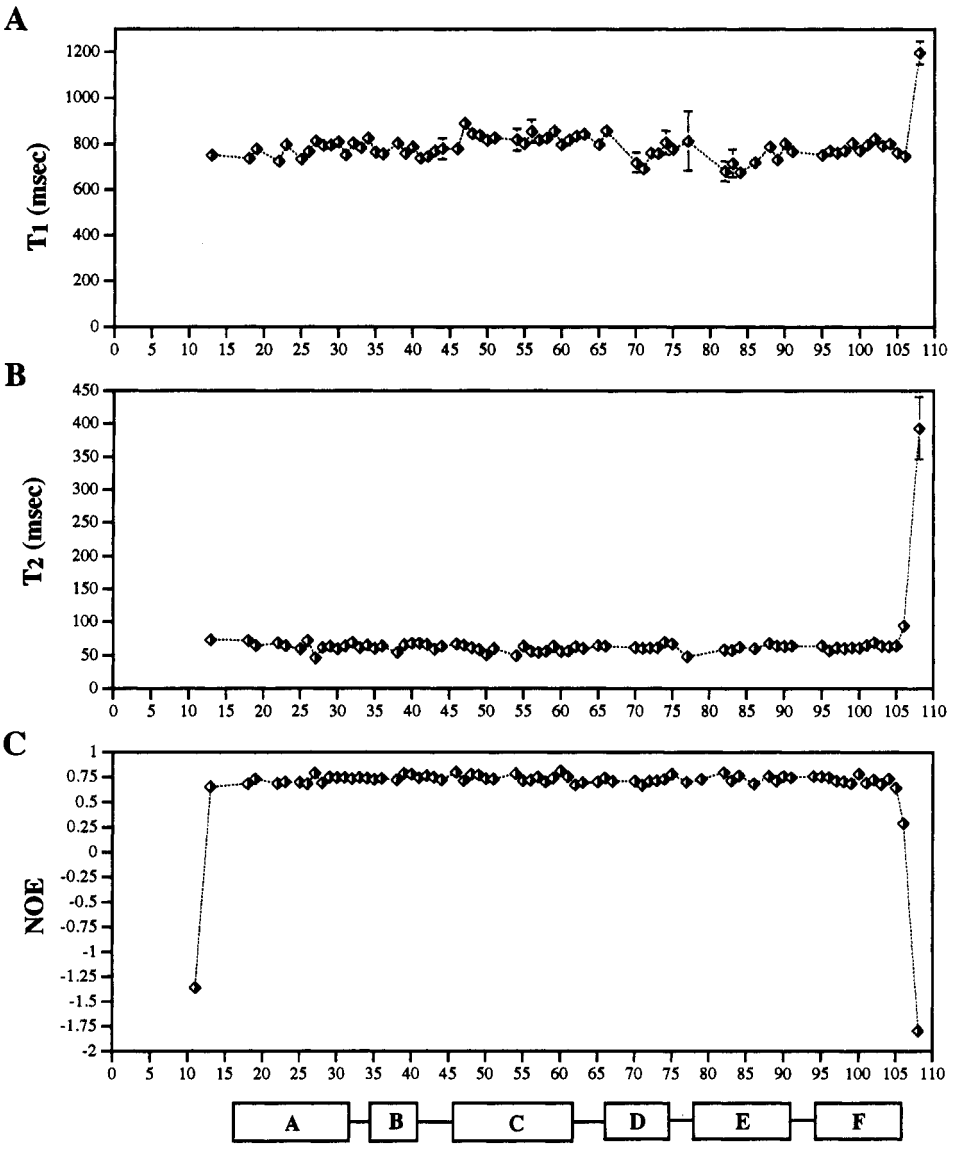

FIGURE 3: Plots as a function of residue number of the measured T_1 (A), T_2 (B), and $\{^1H\}-^{15}N$ NOE (C) values. The secondary structure determined in solution for *trp* repressor (Zhao et al., 1993) is indicated with boxes.

the model-free model of Lipari and Szabo (1982a,b) but in contrast to the latter allows an explicit consideration of anisotropy and presents a clear physical picture of the actual internal motions in the peptide backbone that is consistent with MD simulation.

For each residue the semiangle of the cone (α) and the internal librational correlation time (τ_e) were obtained by minimizing the following merit function $Z(\alpha, \tau_e)$:

$$Z(\alpha,\tau_e) = \left[\frac{T_{1,calc} - T_{1,expt}}{T_{1,calc}}\right]^2 + \left[\frac{T_{2,calc} - T_{2,expt}}{T_{1,calc}}\right]^2 + \left[\frac{NOE_{calc} - NOE_{expt}}{NOE_{calc}}\right]^2 \quad (21)$$

where the $T_{1,expt}$, $T_{2,expt}$, and NOE_{expt} are the experimental values of the relaxation parameters. The $T_{1,calc}$, $T_{2,calc}$, and NOE_{calc} are the calculated values of the relaxation parameters based on eq 1−5 and 16 using the determined $D_{\parallel}$, $D_{\perp}$ values and the variable parameters α and τ_e. The minimization procedure was performed again by using a conjugate gradient method (Press et al., 1989) to find the optimum variable parameters. The optimized α and τ_e values were plotted out in panels A and B of Figure 7 as a function of residue number.

The mean semiangle is found to be 20.9 ± 5.7°. The semiangles for the C-terminal residues D108 and K106 are equal to 61.7° and 31.6°, respectively—much larger than the mean value. This is quite reasonable because the residues on termini are less restricted in their mobility. It is expected that the residues on the N termini should show the same behavior as the C-terminal residues, but unfortunately none of these residues appear in the spectra because their amide proton magnetization is saturated as a result of very rapid solvent exchange. Except for the residues near the protein termini the semiangles for most residues do not show significant variations across the protein backbone. It is interesting to note that the average semiangles for residues in the ABCF hydrophobic core region found to be 20.1 ± 2.5° are almost identical to the those for the DNA-binding DE region of 19.2 ± 4.5°. This confirms the conclusion

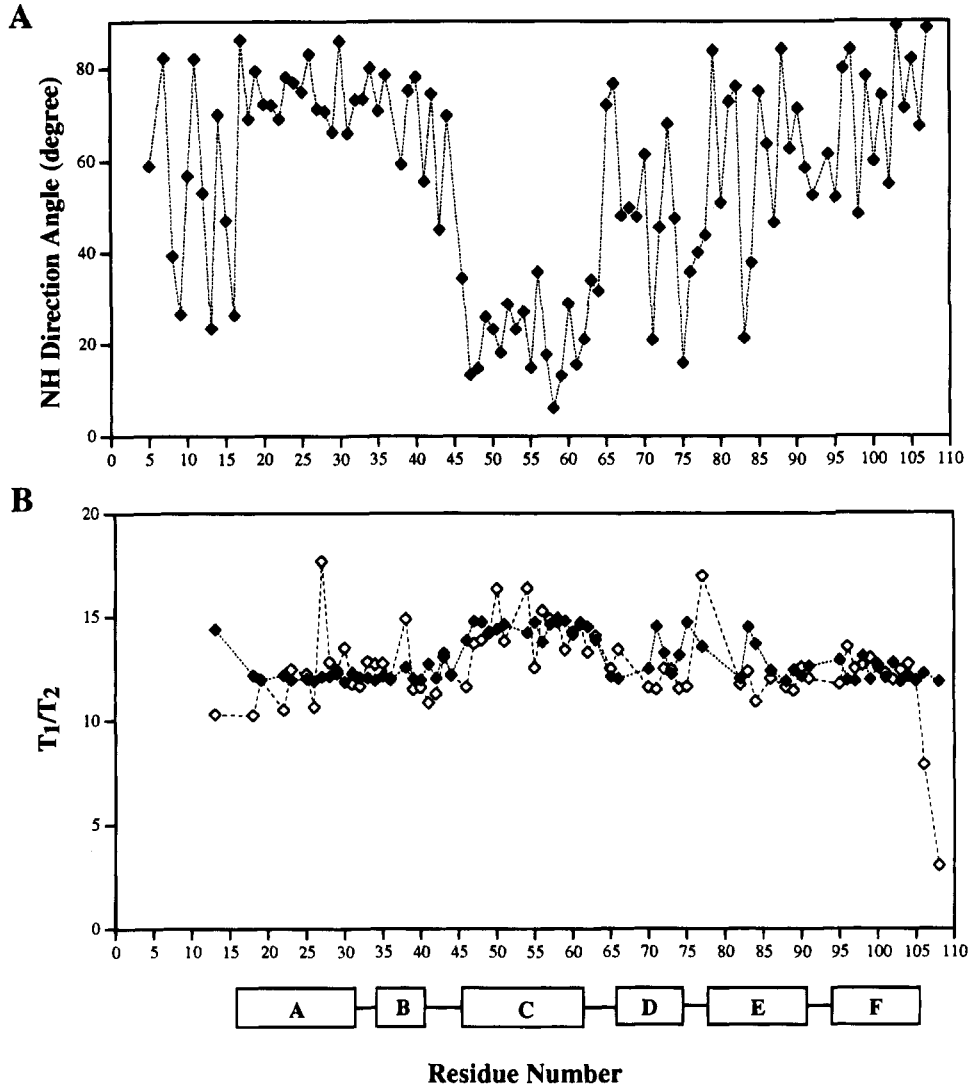

FIGURE 4: Plots as a function of residue number of the angle between the average NH vector and the long axis of the molecule (A) and measured (◇) and calculated (◆) T_1/T_2 values (B). The secondary structure determined in solution for *trp* repressor (Zhao et al., 1993) is indicated with boxes.

that can be drawn from the raw relaxation data, i.e., that on the nanosecond time scale the DE helixes are as rigid as the helixes in the core and the entire protein backbone behaves as a unit. The mean internal correlation time can be estimated to be 21.5 ± 12.2 ps. Similarly to the result of semicone angles, except for the C-terminal residue (D108) the τ_e values for the residues throughout the protein backbone do not deviate significantly from the mean value. It should be noted, however, that the estimates of τ_e should be regarded as qualitative, as we found in the course of performing the minimization procedures that for most residues τ_e is very insensitive to the sum of the least squares function $Z(\alpha,\tau_e)$. Several previous ^{15}N relaxation studies have made a similar observation, i.e., that the internal librational correlation time, τ_e, tends to have large variations with few changes on the other parameters (Palmer et al., 1991; Stone et al., 1992; Cheng et al., 1993). Also shown in Figure 7 is the corresponding order parameter, S^2, or constant A given in eq 10, calculated from the cone angle for each residue. The mean order parameter is found to be 0.81 ± 0.10. The order parameters for all residues except K106 and D108 are above 0.7, leading to the same conclusion that the internal motions on the picosecond scale are very restricted in both the hydrophobic core and the DNA-binding regions, so that the whole molecule is rather rigid on a nanosecond time scale. This finding is important in the light of the previously reported observation that the backbone proton exchange in the DNA-binding region is orders of magnitude faster than in the core (Czaplicki et al., 1991; Gryk et al., 1995), suggesting that the region is more "flexible" than the core. The contrast in the behavior of this segment on the nano- and millisecond time scales makes it necessary to distinguish between "true" or complete flexibility, which would be reflected in both relaxation and proton exchange measurements, and "apparent" or partial flexibility—rather structural instability, which manifests itself only on the longer time scales.

Internal Motion, Disorder, and Flexibility. The root-mean-squared deviation between a series of NMR structures is usually considered as a measure of molecular segmental flexibility. By this criterion, the family of solution structures of the *trp* repressor (Zhao et al., 1993) suggests that the protein shows a higher degree of mobility or flexibility in the helix−turn−helix DNA-binding region than in the hydrophobic core region. This is clearly inconsistent with the results obtained from the ^{15}N relaxation data, as well as

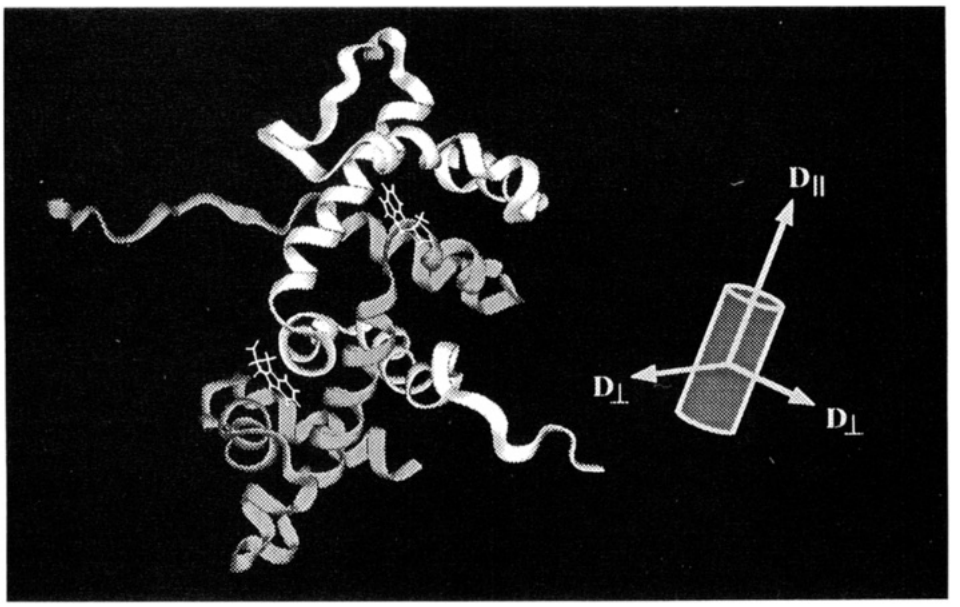

FIGURE 5: Ribbon diagram of one of the *trp* repressor solution structures (Zhao et al., 1993), drawn with the program Insight II (Biosym, San Diego, CA). The two monomers in the structure are represented by lighter and darker ribbons. The axes of the axially symmetric rotational diffusion tensor ($D_{\parallel}$ and $D_{\perp}$) are given schematically in a cylindrical diagram. The unique axis of the diffusion tensor is oriented closely along the two C helices of the dimeric molecule.

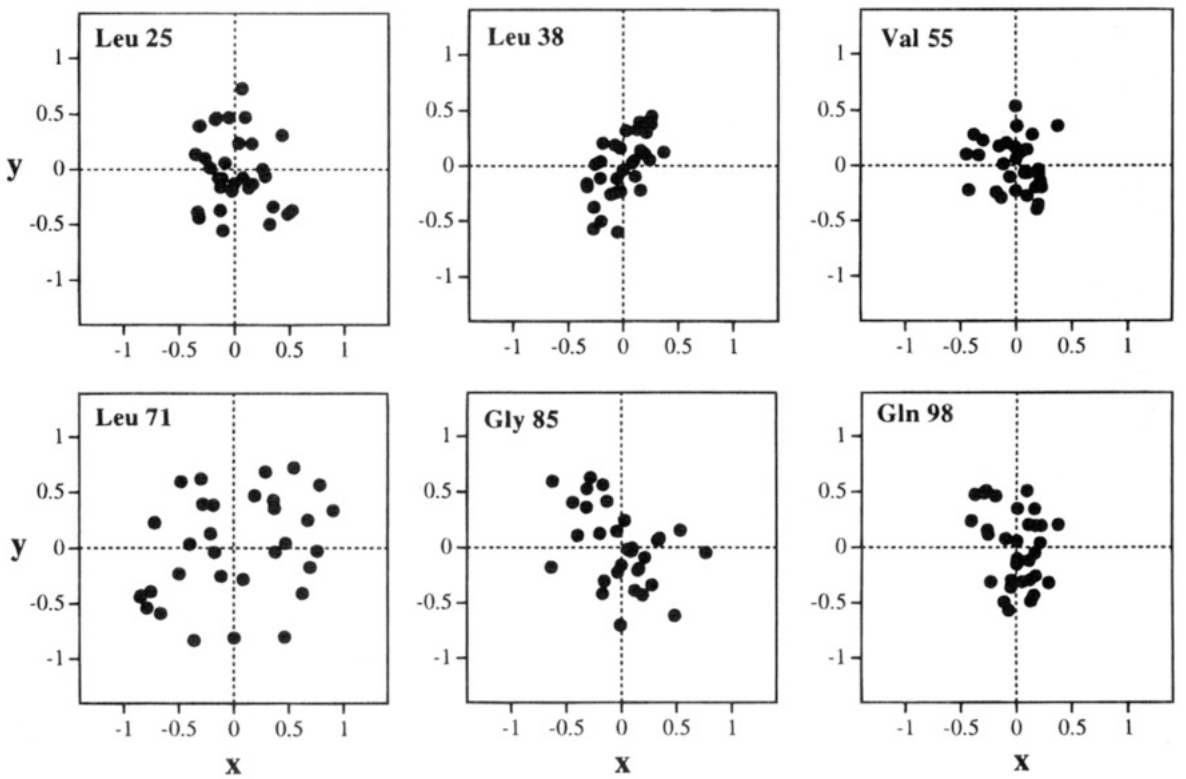

FIGURE 6: Cross sections through the plane perpendicular to the direction of the average NH vector for selected residues in *trp* repressor. The trajectories of NH vectors for each residue illustrate an internal motion pattern for each of the six helices. The NH vectors either form a cone (Leu 25, Val 55, Leu 71, and Gly 85) or a cone whose cross sections are ellipsoidal (Leu 38 and Gln 98).

with chemical shift data which indicate that the DNA-binding region is largely helical (Zhao et al., 1993). But we should keep in mind that the NMR structures are calculated from a set of internuclear NOE constraints between protons in a protein, and "disorder" simply reflects the relative lack of NOE constraints. This may be either due to a higher degree of flexibility in that region *or* due to fast chemical exchange which prevents the NOEs in that region from being observed. In the former case the flexibility should be reflected also in the relaxation behavior; in the latter case it need not. Recent studies of the amide proton solvent exchange rates for *trp* repressor by the proton longitudinal relaxation technique (Gryk et al., 1995; Zheng et al., unpublished results) showed that three types of exchange were observed in different segments of the molecule: (1) slow exchange (on a minute–hour time scale) in the core of the molecule, (2) relatively rapid exchange, with the rates on a proton T_1 relaxation time scale (seconds), in the DNA-binding region, and (3) very fast exchange, at the N and C termini, with rates comparable to the intrinsic exchange rates calculated by the method of

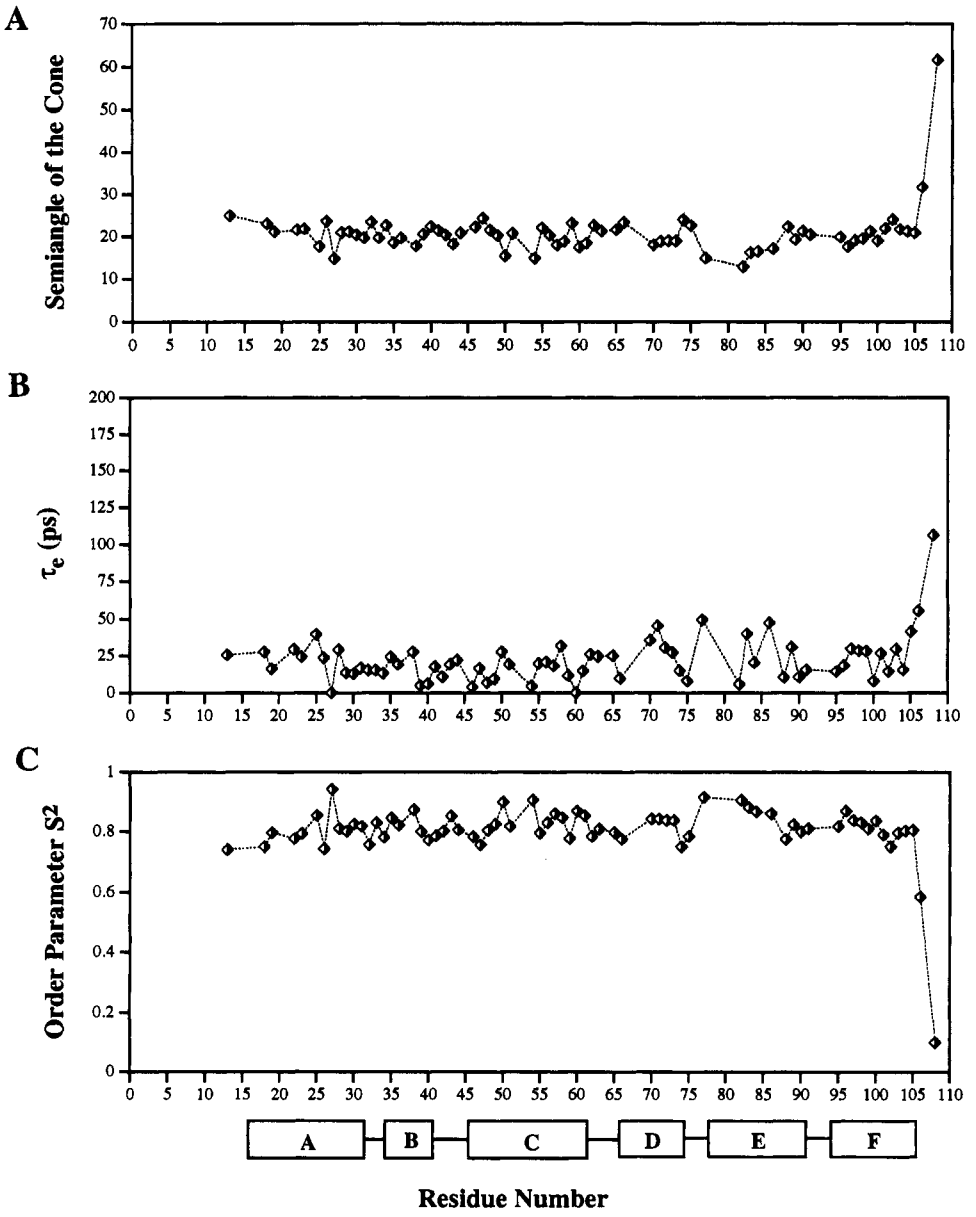

FIGURE 7: Plots of the semiangle of the cone (A), internal correlation time (B), and order parameter (C) as a function of residue number. The secondary structure determined in solution for *trp* repressor (Zhao et al., 1993) is indicated with boxes.

Englander and co-workers (Bai et al., 1993). The contrast between these findings and the relaxation findings reported here allows us to say that the "flexibility" of the *trp* repressor solution structure is apparent rather than real. These studies also suggested that multiple-step conformational exchange processes on the millisecond to second time scale may be involved in the DNA-binding process. Since T_2 was measured with a pulse sequence containing a CPMG (Carr & Purcell, 1954; Meiboom & Gill, 1958) pulse train, the effect of chemical exchange processes occurring on time scales slower than the time between the refocusing pulses in the CPMG sequence is minimized. In any case such effects on T_2 can only be seen if there is averaging between environments with a substantial difference in chemical shift. ^{15}N relaxation measurements reported here will not reflect these interesting slow motions, and thus no substantial differences in the cone−angles and internal correlation times are found between residues in the core of the molecule and in the DNA-binding region. At both N and C termini very fast solvent exchange can be viewed as a consequence of the rapid internal motions and lack of intramolecular hydrogen bonds.

It would be of interest to compare the mobility of *trp* repressor in solution and when crystallized. The degrees of flexibility in the crystal are normally evaluated by the crystallographic temperature *B*-factor. Although called a "temperature factor", it includes not only temperature-dependent vibrations of the protein but also static lattice disorder. The greater the *B*-factor value is, the less localized is the atom in the crystal. A value of 79 Å^2 for the *B*-factor implies an rms vibration of 1 Å. The average *B*-factor value in the DNA-binding domain of the *trp* repressor (Lawson et al., 1988) was reported to be about 22 Å^2, only twice as large as in the central core domain, suggesting that the flexibility for the helix−turn−helix was not significant. However, it was also found (Lawson et al., 1988) that even at identical growth conditions two crystal forms of *trp* repressor (trigonal and orthorhombic) may form, which were found to have distinctly different conformations in the DNA-binding domain. Thus, the large *B*-factor may result from

translocation—and packing disorder—of the DE helices, rather than from internal motion. The profile of segmental motion suggested by the *B*-factor or conformational change between two forms of crystals resembles that of the amide—proton exchange rates (Czaplicki et al., 1991; Gryk et al., 1995) rather than of the semiangles of the cone, indicating that the motions reflected in the crystal for the DNA-binding region occur on a relatively long time scale with correlation times longer than a millisecond. It seems that in different crystals the molecule undergoing such a slow conformational change is locked in one of the possible conformations by the crystal packing forces, and the helix—turn—helix appears well ordered internally, in agreement with the findings reported here.

Anisotropy and Hydrodynamic Behavior. In a previous section, the motional anisotropy of the overall reorientation of the *trp* repressor has been determined from the measured T_1/T_2 values. It is also very interesting to compare the experimental measurements with the existing rigid rotor hydrodynamic models under either stick or slip boundary conditions. Under the stick boundary condition, it is assumed that the rigid particle is immersed in a continuous fluid, and at the surface of the particle the fluid rotates with the particle (i.e., sticks to the particle). Under slip boundary conditions, rotational resistance is a consequence of the displacement of solvent molecules from the volume swept out during the rotation, and the interaction between solvent and solute is assumed to be negligible. In both stick and slip models, the motional anisotropy is solely related to the physical shape of the rigid rotor. The calculation of the rotational diffusion coefficients for the stick model was proposed by Perrin (1934) for an anisotropic ellipsoid and found to be consistent with the results reported later by Favro (1960). The corresponding calculation for the slip model was published by Youngren and Acrivos (1975). Given the axial ratio of 1.61:1.15:1 for *trp* repressor as determined from the solution structures, the ratio of the rotational diffusion coefficients (D_{xx}:D_{yy}:D_{zz}) are found to be 1.38:1.04:1 for the stick model and 12:1.8:1 for the slip model. Although the calculation was based on a relatively crude hydrodynamic model with internal motions being neglected, the ratio of the rotational diffusion coefficients calculated from the Perrin stick model shows reasonable agreement with the ratio of 1.29:1:1 calculated from T_1/T_2 values. This indicates that the *trp* repressor indeed behaves as a very rigid molecule. The large deviation of the results for the slip model from those measured also suggests that interaction between the protein and surrounding solvent cannot be neglected. The calculation shows that our experimental results are consistent with the views in the literature that large molecules are well represented by a stick model while a model under the slip boundary condition better represents small molecules with weak interactions between the solute and solvent (Bauer et al., 1974; Zheng et al., 1993).

In a previous study on the protein backbone dynamics by ^{15}N relaxation (Farrow et al., 1994; Cheng et al., 1993; Barbato et al., 1992), the overall reorientations were found to be approximately isotropic as the difference between the long and short semiaxis of the molecule was small. *Trp* repressor is unique because it has a rather large anisotropy and a relatively rigid backbone. It is an interesting model for the investigation of anisotropic motions. It has been demonstrated in this report that the consideration of anisotropic rotation should be included in the data analysis for molecules with a large axial ratio and that the motional anisotropy can be accurately determined from the ^{15}N relaxation measurements.

CONCLUSIONS

^{15}N T_1, T_2, and NOE experiments indicate that on a nanosecond time scale the *trp* repressor is quite rigid along the whole protein backbone except for the two termini. Comparing this finding with the findings obtained from amide—proton exchange experiments (Czaplicki et al., 1991; Gryk et al., 1995), we may conclude that the DNA-binding region (helices D and E) is unstable on a millisecond time scale but not generally disordered on a time scale reflected in the relaxation measurements. This constellation of findings makes it necessary to distinguish between true flexibilty, reflected in *both* the relaxation and proton exchange measurements, and apparent flexibility—in reality only an instability of the structure—manifested in the latter, but not in the former. The slower motions with correlation times longer than milliseconds may, however, play an important role in protein—DNA recognition, as suggested by the work of Gryk et al. (1995).

ACKNOWLEDGMENT

The authors thank Mr. Michael Gryk for preparing the protein sample and Dr. Daqing Zhao for sharing his structure calculation results. J.C. particularly appreciates the support from Mr. Hideo Haruna.

REFERENCES

Abragam, A. (1961) *Principles of Nuclear Magnetism,* Oxford University Press (Clarendon), London.
Arrowsmith, C. H., Carey, J., Treat-Clemons, L., & Jardetzky, O. (1989) *Biochemistry 28,* 3875—3879.
Arrowsmith, C. H., Pachter, R., Altman, R. B., Iyer, S., & Jardetzky, O. (1990) *Biochemistry 29,* 6332—6341.
Arrowsmith, C. H., Czaplicki, J., Iyer, S. B., & Jardetzky, O. (1991a) *J. Am. Chem. Soc. 113,* 4020—4022.
Arrowsmith, C., Pachter, R., Altman, R., & Jardetzky, O. (1991b) *Eur. J. Biochem. 202,* 53—66.
Bai, Y., Milne, J. S., Mayne, L., & Englander, S. W. (1993) *Proteins: Struct., Funct., Genet. 17,* 75—86.
Barbato, G., Ikura, M., Kay, L. E., Pastor, R. W., & Bax, Ad. (1992) *Biochemistry 31,* 5269—5278.
Bauer, D. R., Brauman, J. I., & Pecora, R. (1974) *J. Am. Chem. Soc. 96,* 6840—6843.
Borden, K. L. B., Bauer, C. J., Frenkiel, T. A., Beckmann, P., & Lane, A. N. (1992) *Eur. J. Biochem. 204,* 137—146.
Carr, H. Y., & Purcell, E. M. (1954) *Phys. Rev. 94,* 630—638.
Cheng, J., Lepre, A. C., Chambers, S. P., Fulghum, J. R., Thomas, J. A., & Moore, J. M. (1993) *Biochemistry 32,* 9000—9010.
Czaplicki, J., Arrowsmith, C., & Jardetzky, O. (1991) *J. Biomol. NMR 1,* 349—361.
Farrow, N. A., Muhandiram, R., Singer, A. U., Pascal, S. M., Kay, C. M., Gish, G., Shoelson, S. E., Pawson, T., Forman-Kay, J. D., & Kay, L. E. (1994) *Biochemistry 33,* 5984—6003.
Favro, L. D. (1960) *Phys. Rev. 119,* 53—62.
Gryk, M. R., Finucane, M. D., Zheng, Z., & Jardetzky, O. (1995) *J. Mol. Biol. 246,* 618—627.
Hiyama, Y., Niu, C.-H., Silverton, J. V., Bavoso, A., & Torchia, D. A. (1988) *J. Am. Chem. Soc. 110,* 2378—2383.
Howarth, O. W. (1978) *J. Chem. Soc., Faraday Trans. 2 74,* 1031—1041.
Howarth, O. W. (1979) *J. Chem. Soc., Faraday Trans. 2 75,* 863—873.
Kay, L. E., Torchia, D. A., & Bax, A. (1989) *Biochemistry 28,* 8972—8979.

King, R., & Jardetzky, O. (1978) *Chem. Phys. Lett. 55,* 15−18.
King, R., Maas, R., Gassner, M., Nanda, P. K., Conover, W. W., & Jardetzky, O. (1978) *Biophys. J. 24,* 103−117.
Kitamaru, R. (1986) in *Applications of NMR Spectroscopy to Problems in Stereochemistry and Conformational Analysis* (Takeuchi, Y., & Marchand, A. P., Eds.) pp 75−124, VCH Publishers, Inc., London.
Klig, L. S., Carey, J., & Janofsky, C. (1988) *J. Mol. Biol. 202,* 769−777.
Lawson, C. L., Zhang, R., Schevitz, R. W., Otwinowski, Z., Joachimiak, A., & Sigler, P. B. (1988) *Proteins: Struct., Funct., Genet. 3,* 18−31.
Lipari, G., & Szabo, A. (1982a) *J. Am. Chem. Soc. 104,* 4546−4559.
Lipari, G., & Szabo, A. (1982b) *J. Am. Chem. Soc. 104,* 4559−4570.
Luisi, B. F., & Sigler, P. B. (1990) *Biochim. Biophys. Acta 1048,* 113−126.
Marion, D., & Wüthrich, K. (1983) *Biochem. Biophys. Res. Commun. 113,* 967−974.
Meiboom, S., & Gill, D. (1958) *Rev. Sci. Instrum. 29,* 688−691.
Otwinowski, Z., Schevitz, R. W., Zhang, R.-G., Lawson, C. L., Joachimiak, A., Marmorstein, R. Q., Luisi, B. F., & Sigler, P. B. (1988) *Nature 335,* 321−329.
Pabo, C. O., & Sauer, R. T. (1992) *Annu. Rev. Biochem. 61,* 1053−1095.
Palmer, A. G., Rance, M., & Wright, P. E. (1991) *J. Am. Chem. Soc. 113,* 4371−4380.
Paluh, J. L., & Yanofsky, C. (1986) *Nucleic Acids Res. 14,* 7851−7860.
Perrin, F. (1934) *J. Phys. Radium 10,* 497−511.
Press, W. H., Flannery, B. P., Teukolsky, S. A., & Vetterling, W. T. (1989) *Numerical Recipes*, Cambridge University Press, Cambridge.
Remesh, V., Frederick, R. O., Syed, S. E. H., Gibson, C. F., Yang, J., & Roberts, G. C. K. (1994) *Eur. J. Biochem. 225,* 601−608.
Schevitz, R. W., Otwinowski, Z., Joachimiak, A., Lawson, C. L., & Sigler, P. B. (1985) *Nature 317,* 782−786.
Shaka, A. J., Keeler, J., & Freeman, R. (1983) *J. Magn. Reson. 53,* 313−340.
Stone, M. J., Fairbrother, W. J., Palmer, A. G., Reizer, J., Saiser, M. H. J., & Wright, P. E. (1992) *Biochemistry 31,* 4394−4406.
Woessner, D. E. (1962a) *J. Chem. Phys. 36,* 1−4.
Woessner, D. E. (1962b) *J. Chem. Phys. 37,* 647−654.
Youngren, G. K., & Acrivos, A. (1975) *J. Chem. Phys. 63,* 3846−3848.
Zhang, H., Zhao, D., Revington, M., Lee, W., Jia, X., Arrowsmith, C. H., & Jardetzky, O. (1994) *J. Mol. Biol. 238,* 592−614.
Zhang, R.-G., Joachimiak, A., Lawson, C. L., Schevitz, R. W., Otwinowski, A., & Sigler, P. B. (1987) *Nature 327,* 591−597.
Zhao, D., & Jardetzky, O. (1993) *J. Phys. Chem. 97,* 3007−3012.
Zhao, D., & Jardetzky, O. (1995) in *Adaptation of Simulated Annealing to Chemical Problems* (Kalivas, J. H., Ed.) Elsevier Science, Amsterdam, The Netherlands (in press).
Zhao, D., Arrowsmith, C. H., Jia, X., & Jardetzky, O. (1993) *J. Mol. Biol. 229,* 735−746.
Zheng, Z., Mayne, C. L., & Grant, D. M. (1993) *J. Magn. Reson. A103,* 268−281.

BI942689O